PAPER

Check for updates

Elucidating the mechanism of nucleation inhibition of pathology crystallization of gout based on the evidence from amorphous form and in solution†

Dan Zhou,‡ Shiqi Jiao, Pengfei Zhang,‡ Yige Jin, Yonglan Pan, Chunyan Ou, Xingde Zhang, Tingming Fu and Yonghai Liu [ID] *

The first gout attack in a hyperuricaemic patient may be regarded as a nucleation event which is caused by monosodium urate monohydrate (MSUM) deposition in the synovial fluid. The effect of Tailor-Made Inhibition (TMI) may be effective as drugs for the prevention of aberrant nucleation and crystallization. Therefore, the understanding of the underlying mechanisms in inhibiting the MSUM nucleation by TMI has proven to be of great significance. Yet most of the published studies about nucleation inhibition have tended to focus on simpler molecular models with a hydrogen-bonded acceptor and donor, which may be not suitable for the uric acid molecule with multiple hydrogen-bonded acceptors and donors under physiological conditions. Herein, the mechanisms of nucleation inhibition of MSUM were explored in a simulated biological environment (0.15 M Na$^+$ and pH 7.40) in the presence and absence of TMI. And the evidence of nucleation inhibition by TMI in solution and the amorphous form of MSUM was investigated by HNMR, IR, Raman, PXRD, Dynamic light scattering (DLS), induction time measurements, and density functional theory (DFT) calculations. Results showed that the inhibition comes from a combination of kinetic and thermodynamic effects, with an impact of kinetics as the TMI inhibition effects far exceeded what could be accounted for by changes in usual factors of classical nucleation theory. The data demonstrated that the complex between urate and TMI disturbed the formation of two-dimensional sheets of sodion and purine rings parallel to the (011) plane and further impeded the formation of a three-dimensional structure with aromatic stacking interactions in solution. To our knowledge, the nucleation inhibition of TMI is achieved by suppressing interplanar stacking, which is a mechanism proposed for the first time.

Introduction

Gout, a crystal-induced arthritis connected with hyperuricemia, is a kind of severe joint disease and prevailingly occurs in the big toe, ankles, and knees; it is very commonly caused by the deposition of MSUM in the synovial fluid.[1,2] The effect of TMI on the nucleation process has been an area of growing focus,[3] since TMI may be effective as drugs for the prevention of aberrant nucleation and crystallization.[4,5] Therefore, MSUM mimics, as the candidate drug molecules, may provide a rational strategy for the prophylaxis of acute gout attack and treatment of tophus in the context of hyperuricemic patients. As a result, the fundamental and theoretical understanding of the underlying mechanisms in inhibiting the MSUM nucleation by TMI has proven to be of great significance. Yet most of the published studies about nucleation inhibition,[6–8] to the knowledge of the authors, have tended to focus on simpler molecular models with a hydrogen-bonded acceptor and donor, which may be not suitable for uric acid molecules with multiple hydrogen-bonded acceptors and donors under physiological conditions.

Recently, we report that the growth of MSUM crystals was strongly modulated by additives or different ions.[9] Particularly, xanthine, a TMI of uric acid, could strongly inhibit the growth of MSUM, indicating that MSUM solubility and precipitation may be modulated by local and systemic biological environments.[10]

In this study, we focused on uncovering inhibition mechanisms of xanthine on MSUM nucleation based on the evidence from amorphous form and in solution, which is determined by induction time measurements and other combined experimental identification (DLS, HNMR, IR, Raman, PXRD, DFT calculations).

Experimental

Measurement of induction time and design of experiments

The induction times of MSUM nucleation from solutions in the absence/presence of xanthine were measured at 15 °C. Each

School of Pharmacy, Nanjing University of Chinese Medicine, Nanjing 210046, China. E-mail: liuyh@njucm.edu.cn

‡ These authors contributed equally to this work.

experiment for induction time was carried out in a 100 mL glass jacketed beaker at 15 °C. In each run, a 50 mL MSUM solution was prepared in a properly capped glass bottle at an elevated temperature of 95–97 °C, in a given concentration and additive. This solution was kept agitated at 95–97 °C for 20 min to make sure all solids were totally dissolved. And it was quickly transferred to a 100 mL jacketed beaker controlled at 15 °C, agitating with a magnetic stirrer at 60 rpm. And the solution was recorded by a high definition web camera. The onset of nucleation was surveyed as a very rapid change from a clear to a cloudy solution. The induction time was defined as the period from the moment at which the solution was transferred to the 100 mL beaker to the moment at which the cloud point was identified. The distribution of induction times in this study can be analyzed using eqn (1) to determine the time-independent nucleation rate of the experimental system.

$$\ln(1 - P(t)) = -JV(t - t_g) \tag{1}$$

where $P(t)$ is the probability to be formed in an experiment after an elapsed time of t. The $P(t)$ is obtained from the distribution of experimental induction times.[7,11] The volume of the crystallizing solution of sample is V, and the nucleation rate is J, and t_g is the time required for a crystal to grow to a detectable size.[7] Meanwhile, the representative induction time of an experiment is equal to $(JV)^{-1}$.

Solubility measurement

The solubility of MSUM in water was measured after 72 hours of crystal cultivation at 15 °C and at pH = 7.4. Supersaturated solutions of different concentrations of MSUM were made by adding a known amount of solute and 100 mL water in a beaker. The beakers were placed in the drying oven at a temperature of 15 °C for 72 hours. And the MSUM crystal appeared after 72 hours of cultivation. The drying oven and suction filter device were utilized to obtain dry crystals. The solubility was obtained by subtracting the mass of the acquired crystal from the mass of solute. Moreover, a certain amount of xanthine were added to the standard MSUM solution, respectively. For the standard MSUM solution, the concentration of MSUM was 8 mM and that of sodium chloride was 150 mM. The obtained crystals of sample were handled in the same way as them to acquire the solubility.

Characterization method

The DLS experiments were conducted at 37 °C, which was controlled by a Grant LTD-6 water bath system. The samples were measured on a Malvern Zetasizer Nano ZS90 zeta (USA). ^{1}H NMR were measured on a Bruker AM 600 MHz spectrometer. Fourier transform infrared spectroscopy of sample was employed to be characterized by a Bruker Alpha FTIR-ATR instrument in 4 cm^{-1} resolution with a 4000–400 cm^{-1} range. Raman spectroscopy was used to characterize the structure of MSUM and a ReactRaman 0163 instrument scanned the sample from 3200 to 100 cm^{-1} for three times. The samples of amorphous MSUM were obtained by the same procedure as the

nucleation experiments, and the sample collection time was set to the induction time based on the results of the measurement of Induction Time. And the wet sample was instantly characterized by PXRD, IR and Raman in order to avoid any effects of the phase transition. All experiments were run three times.

Computational details of DFT

(1) Quantum chemical calculations. DFT calculations have been performed by using a Gaussian 09 package.[12] Binding energies of the complexes are calculated using a B3LYP functional. A Gaussian-type 6-311++G(d,p) basis set is utilized for geometry optimization and accounted for solvent effects by the solvation model based on density (SMD). The binding energy of complex is defined as:

$$E_{BE} = E_{purine1^- + 2cation^+ + purine2^-} - E_{purine1^-} - 2E_{cation^+} - E_{purine2^-}$$

where E_x represents the total electronic energy of species x.

(2) Natural bond orbital (NBO) partial atomic charges. NBO partial atomic charges was made by using a Gaussian 09 package based on the optimized molecule, and it is calculated by a B3LYP functional. A Gaussian-type 6-311++G (d, p) basis set is utilized for geometry optimization and accounted for solvent effects by the SMD solvation model.

(3) ^{1}H NMR chemical shifts. NMR chemical shifts was made by using a Gaussian 09 package on the basis of the optimized molecule, and it is calculated using a B3LYP functional. A Gaussian-type 6-311++G (d, p) basis set is utilized for geometry optimization. And ^{1}H NMR chemical shifts are calculated using the B3LYP functional with a Gaussian-type 6-311++G (d, p) basis set.

Results and discussion

Solubility

The solubility of MSUM in the presence of 150 mM NaCl, 8 mM urate, and xanthine at 15 °C (experimental conditions) was measured in this study and presented in Fig. S1.† The solubility increases significantly with the increase in the concentration of xanthine, showing that xanthine has a great salting-in effect on MSUM, which appears to be an expected trend and consistent with our previous report.[10,13,14]

Induction time theory and results

Induction time measurements of MSUM in different concentrations of solutions were primarily performed at a temperature of 15 °C in the absence/presence of xanthine. The stochastic nature of MSUM nucleation can be investigated and analyzed from these large data sets *via* cumulative probability distributions (CPD) of induction times.[15] $P(t)$ is the probability to be formed in an experiment after an elapsed time of t.

$$P(t) = 1 - \exp(-JV(t - t_g)) \tag{2}$$

The value of t_g is neglected given that it is often very small compared to the time scale of t.[7,14] In this study, for the measurements, the validity of this assumption was confirmed

by utilizing the image-capture data from the nucleation experiments.

Supersaturation in this work is defined in eqn (3).

$$S = c/c^* \qquad (3)$$

In eqn (3), S is the reported supersaturation, c is the dissolved concentration of MUSM in water including 150 mM NaCl (pH = 7.4) in the absence/presence of xanthine, and c^* is the saturation concentration of MSUM in water including 150 mM NaCl (pH = 7.4) in the absence/presence of xanthine. To compensate for shifts in solubility in the presence of xanthine, and an adjusted excess amount of MSUM had to be added to samples that contained xanthine to ensure that every experiment was carried out at a constant supersaturation, thereby ensuring that the measured results could be compared with respect to a common set of baseline conditions. And the effect of adjusting the supersaturation in the presence of xanthine is reflected in Fig. 1 and Table 1. The data demonstrate the expected behavior of monotonically decreasing nucleation rates with reducing supersaturation.

The nucleation rate information was shown in Fig. 2. The resulting correlations provided good fits for the nucleation rate data and promoted the estimation of the representative pre-exponential factor (A) and activation energy (B) constants for the two systems with and without TMI. And the values shown in Table 2, indicate an increase in both A and B parameters for the nucleation experiments in the presence of TMI. The calculated increase in B is about approximately 57% with respect to that of the no TMI system, which seems like a reasonable conclusion

Table 1 Results of induction time experiments as a function of S, including 95% confidence intervals from linear regression

Sample[a]	S[b]	J (m^{-3} s^{-1})	τ (s)	Sample[c]	S	J (m^{-3} s^{-1})	τ (s)
7.9 mM	47.0	198	101	2% TMI	46.8	118	170
7.7 mM	45.8	174	115	6% TMI	46.1	88	227
7.5 mM	44.6	150	133	10% TMI	44.3	72	278
7.3 mM	43.5	120	167	14% TMI	43.4	56	357

[a] Sample is a solution of different concentrations of urate at pH = 7.4 in the presence of 150 mM NaCl. [b] S is the supersaturation. [c] Sample is a solution of different concentrations of xanthine at pH = 7.4 in the presence of 150 mM NaCl and 8 mM urate.
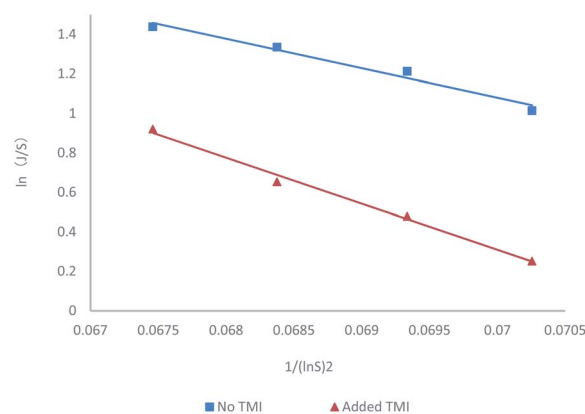

Fig. 2 Nucleation kinetics as a function of concentration ratio (S), as predicted by the classical nucleation correlation, including 95% confidence intervals from linear regression. Nucleation rates are consistently slower upon the addition of a small amount of TMI.
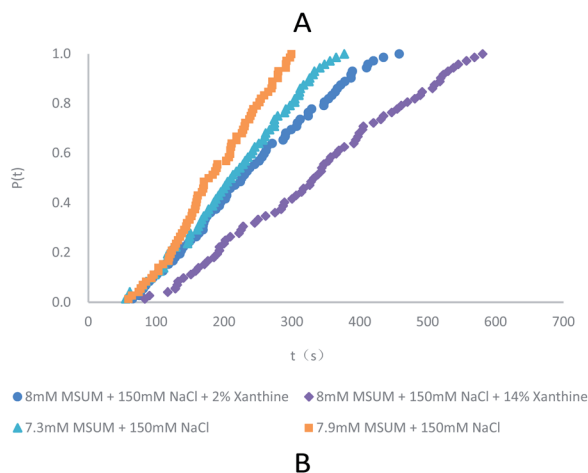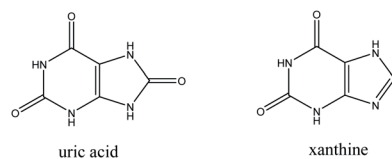

Fig. 1 (A) Molecular structure of uric acid and xanthine. (B) Probability distributions of the induction times in the presence of different concentrations of MSUM and different concentrations of xanthine (note: for clarity, the data in the third and fourth rows of the Table 1 are not plotted).

since the increase in B should theoretically decrease the nucleation rate. However, the change in the pre-exponential parameter A is striking, considering the nearly 20 fold increase in the value of A in the presence of TMI.

The pre-exponential parameter A is defined by Classical nucleation theory[15] in eqn (4).

$$A = (4\pi/3v_0)^{1/3}(\gamma_{\text{ef}}/k_{\text{b}}T)^{1/2}DC_{\text{e}} \qquad (4)$$

In eqn (4), v_0 is the volume of the solute molecules in the crystal phase, γ_{ef} is the effective interfacial energy, D is the diffusivity constant of the solute in the solvent system, k_{b} is the Boltzmann's constant, T is the crystallization temperature, and C_{e} is the solubility. As the experimental data show, the only parameters that could be potentially affected by the TMI are the interfacial energy γ_{ef} and the diffusivity D. However, the γ_{ef} increase only 1.2 folds in presence of TMI, which is minimal (Table 2). So, it is unreasonable to expect that the diffusivity of the crystallizing solute would change by nearly 20 folds due to the presence of the TMI. And it becomes clear that classical nucleation theory cannot rationalize the great changes of MSUM in nucleation rate and kinetics observed by the presence of TMI.[16]

Table 2 Results of kinetic analysis of the nucleation rate data. The reported range for the pre-exponential factor accounts for the error in $\ln(A)$ and represents the calculated 95% confidence interval

Sample	A (s^{-1} m^{-3})	B	γ_{ef}[a] (J m^{-2})	Sample	A (s^{-1} m^{-3})	B	γ_{ef} (J m^{-2})
No TMI	9.89×10^5	148.89	0.02403	With TMI	1.63×10^7	232.85	0.02789

[a] γ_{ef} is the effective interfacial energy.

DLS detection

We recently demonstrated that clusters or "nucleation precursors" existing in MSUM solutions could be dramatically stable with the assistance of additive cations based on the DLS test results.[14] Along the same lines, DLS experiments were also used to investigate the nucleation of MSUM in presence of xanthine (Fig. S2†). And the notable is the fact that the average particle size, after the addition of xanthine with a concentration of 1 mM (concentration of control sample is 10 mM MSUM in the absence of xanthine), obviously decreased from 750 nm to 520 nm. This result confirmed the existence of clusters or "nucleation precursors" which could be dramatically stable and smaller with the assistance of additive TMI. This data appears to be reasonable since the nucleation in the system with xanthine needs to surmount a higher energy barrier, given that total Gibbs free energy in the nucleation process is the competitive outcome between bulk energy and interfacial energy.

DFT calculations on binding energies of solute–solute and solute-TMI in presence of sodion

The crystal structure ($P\bar{1}$; $a = 10.888$ Å, $b = 9.534$ Å, $c = 3.567$ Å, $\alpha = 95.06°$, $\beta = 99.47°$, $\gamma = 97.17°$) of MSUM has been reported from the 1970s. The urate anions interact by virtue of hydrogen bonding and coordinate with the sodium ion through short Na/O electrostatic interactions to form two-dimensional sheets of purine rings parallel to the dominant (011) plane of MSUM (Fig. 3A). Our previous work confirmed that not xanthine but its negative ion could act as an inhibitor at pH = 7.4 to suppress the MUSM crystallization.[10] Furthermore, our recent report demonstrated that the nucleation rate of MSUM increased significantly with increasing sodium ion concentration.[14] As a result, based on the analysis of the electrostatic potential distribution of urate and xanthine ion (Fig. S3†), a series of structures of dimers in solute–solute and solute-TMI in presence of sodion were optimized and their binding energies were calculated (Fig. S4 and S5†). As shown in Fig. 3, for the most favorable conformation of dimer in the solute–solute system (FCSS) (the ball urate a and b displayed in Fig. 3A and B), on the basis of the negative E_{BE} values (Fig. S4A†), is formed by the interaction of two head-to-tail chain bridges (urate$^-$···Na$^+$···urate$^-$) and two intermolecular hydrogen-bonding (N–H···O). And secondarily favored conformation is formed by the interaction of two head-to-head chain bridges (urate$^-$···Na$^+$···urate$^-$) (the ball urate b and c displayed in Fig. 3A and C). As a result, by virtue of these two docking modes, urate and sodium ions could bind into a stable planar structure in solution, since a sodium ion can be paired with multiple oxygen
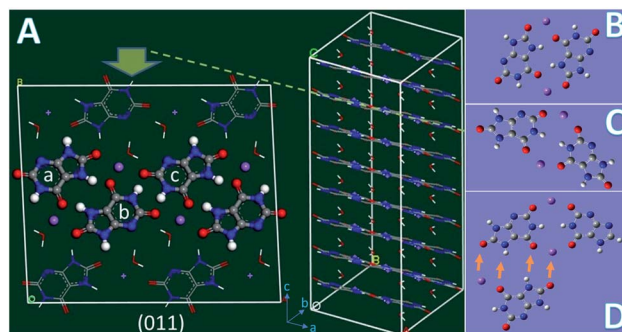

Fig. 3 (A) The (011) plane of the crystal structure of MSUM showing the top view along the c axis (note: the docking conformation between balls urate a and b is similar to the FASS structure, and the docking conformation between balls urate b and c is similar to their secondarily favored conformation in the solute–solute system). (B) The most favorable conformation of dimer in the solute–solute system (FCSS). (C) The secondarily favorable conformation of dimer in the solute–solute system. (D) The most favorable conformation of dimer in the solute-TMI system (FCST). Meanwhile, a foreign urate with a Na ion is docking into FCST (as shown in the direction of the arrow), suggesting that a plane will be spread by the combination of FCST and FCSS.

atoms at the same time. Very interestingly, these two pairing structures really dominate almost the whole major (011) face of MSUM (The ball urate in a···b and b···c displayed in Fig. 3A).[17] Hence, it could be inferred that those optimum conformations may increase in solution as the major "growth units" with increasing of sodium ion concentration, thus leading to the promotion of nucleation by sodium ions. Meanwhile, the most favorable conformation of dimer in the solute-TMI system (FCST) is formed by the interaction of two head-to-head chain bridges (urate$^-$···Na$^+$···urate$^-$), showing that the solute may have a higher affinity with TMI than itself by comparing the difference in negative E_{BE} values (Fig. S5A† and 3D). These results may reasonably explain that xanthine could strongly inhibit MSUM nucleation because it could effectively suppress the major growth units of MSUM. Furthermore, as shown in Fig. 3D, it's interesting to note that xanthine can only inhibit the growth of FCST in a specific direction, so FCST could continue to develop into a planar in other directions by binding with foreign urates and Na ions. Therefore, this direction-specific inhibition effect also could effectively explain why the cluster size is reduced.

HNMR

^{1}H chemical shift is sensitive to subtle changes in the local environment of a molecule, and it is usually used to study

Table 3 Different chemical shifts of protons of C-8 in xanthine in NMR spectrum for samples of diverse ratios of MSUM to xanthine

The molar ratio of MSUM to xanthine	2 : 1	1.5 : 1	1 : 1	1 : 2	0
Chemical shifts of protons of C-8 (ppm)[a]	7.394	7.388	7.385	7.383	7.372

[a] NMR spectrum of 0.08 M xanthine in presence of diverse concentrations of MSUM at 45 °C in D_2O (pH = 7.4, adjusted by NaOH).

Table 4 Different chemical shifts of protons of C-8 in xanthine based on the DFT calculations

Sample	Xanthine	Xanthine ion	FCST	Xanthine solution at pH = 7.4[a]	FCST and xanthine[b]
Chemical shift of H(8) in xanthine	7.510	7.380	7.530	7.449	7.519

[a] A solution consisting of 46.8% xanthine ion and 53.2% un-ionized xanthine molecule (xanthine molecule and xanthine ion content based on calculations of pK_{a1} values of xanthine at pH = 7.4). [b] A solution consisting of 46.8% FAST and 53.2% un-ionized xanthine molecule based on the assumption that all urate ions are docked by xanthine ions (xanthine molecule and xanthine ion content based on calculations of pK_{a1} values of xanthine at pH = 7.4).

molecular association in solution.[18] Based on the investigation of FCST structure, urate and xanthine are almost located in the same plane, which leads to xanthine being in the nuclear magnetic de-shielding field of urate. Therefore, on the one hand, the samples in presence of different concentrations of xanthine were investigated by HNMR and the results showed that the chemical shift of H(8) (Fig. S3†) did not change with the concentration of xanthine. On the other hand, pre-mixed samples of different ratios of MSUM to xanthine were investigated by HNMR (Table 3), and remarkable lower-field proton shifts, associated with increasing the mole ratio of MSUM to xanthine, were observed from the chemical shifts of the C-8 protons of xanthine in D_2O. Hence, this result is consistent with the structural features of FCST obtained from DFT calculations, showing the presence of a de-shielding effect, resulting from the de-shielding field of the urate, which markedly increased along with the improvement of the mole ratio of MSUM to xanthine in solution.

DFT calculations on chemical shifts of HNMR

Quantum-chemical calculations have become highly important tools in the usually difficult assignment of experimental NMR spectra.[19,20] The chemical shifts of H(8) of xanthine, xanthine ion, and xanthine in FCST were investigated by DFT calculation method. As shown in Table 4, in an aqueous xanthine (pK_{a1} = 7.53) solution at pH = 7.4 (note: about 46.8% mol of xanthine ionized at pH = 7.4), the calculated values of HNMR (δ = 7.449) deviated by only about 1% when comparing the detection values (δ = 7.372). And the results of these calculations further demonstrate that FCSTs exist in the solution, and they cannot dominate the entire solution environment but exert a significant inhibitory effect.

Detection of the amorphous form of MSUM in presence of TMI by FTIR, Raman spectra, and PXRD

In this study, we focused on the amorphous form that appeared before the formation of crystals of MSUM, since it may be obtained the critical information in nucleation and crystal

growth.[21] The FTIR and Raman spectra were employed to probe the structures of the crystal form of MSUM and the amorphous form in the absence/presence of TMI, and the results are shown in Fig. 4A–C and D, respectively. And the structural difference of the three can be carefully studied in the three vibrational regions of IR peaks.[17,22,23] Firstly, the oxygen–sodium peaks of MSUM is located at 450–600 cm^{-1}. Secondly, the vibration peak at 787 cm^{-1} of the MSUM represents the –NH– in purine rings. Thirdly, the peaks at 1647 cm^{-1} corresponds to the –OH vibration of water molecules. Moreover, the corresponding symmetrical vibration Raman peaks of the MSUM can be found at 1011, 1062, and 1208 cm^{-1}. As can be seen in Fig. 4, on the one hand, the structural difference between the MSUM and amorphous form without TMI can be inspected in the three vibrational regions of IR peaks. And those peaks of the amorphous form in absence of TMI at 450−600 cm^{-1}, 787 cm^{-1}, and 1647 cm^{-1} all display a red shift in comparison to the
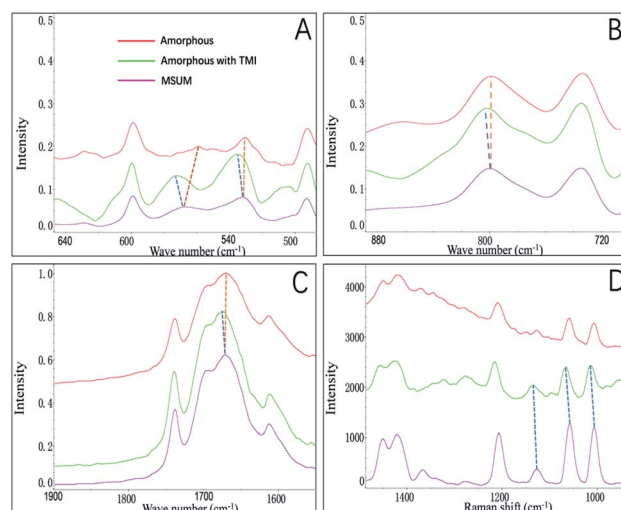

Fig. 4 FTIR spectra details of amorphous form of MSUM in the absence/presence of TMI. (a) The oxygen-sodium peaks, (b) the –NH– peaks, (c) the –OH peaks of water molecules, and (d) Raman spectra details of amorphous form of MSUM in the absence/presence of TMI.

corresponding peak position of MSUM crystal.[17] And on the other hand, those peaks from the samples of amorphous form in presence of TMI all present a blue shift in comparison to the corresponding peak position of MSUM crystal. Meanwhile, the similarly symmetrical vibration Raman peaks of the amorphous phase in presence of TMI all exhibit different degrees of the shift to higher wavenumber in comparison to the corresponding peak position of MSUM crystal and its amorphous phase (Fig. 4D). As a result, these interesting results confirm the following three facts.[17,24] Firstly, the amorphous phase in presence of TMI exhibited a weaker ionic bond between sodium and oxygen (blue shift in 450–600 cm^{-1}). Secondly, intermolecular interactions between purine rings on the plane (011) were changed (blue shift in 787 cm^{-1}). Thirdly, the structures of the amorphous phase in presence of TMI had different water contents, and both the hydrogen bonding between water and purine molecules were weakened (blue shift in 1647 cm^{-1}).

Recently, the transition process over time from an amorphous structure to a crystalline structure was presented by the time-resolved detection of PXRD.[17] The first diffraction peak appears at 28.18° corresponding to the (011) face, and the following developments are the diffraction peaks at 33.70, 18.87, and 11.68°, which correspond to (−2−21), (020) and (1−10) faces. This data showed that an MSUM crystalline structure initially takes place on a dominant two-dimensional (011) face, then spreads out to form a three-dimensional crystal structure by aromatic stacking interactions, as evidenced by the formation of (−2−21), (020) and (1−10) faces. Here PXRD was also used to distinguish the difference in the amorphous phase in the presence/absence of TMI, since the amorphous form as a transition state may provide valuable clues about nucleation and crystallization in presence of additives.[25] As shown in Fig. 5, PXRD patterns showed that xanthine did not change the lattice structure of the amorphous phase of MSUM at 6 mM MSUM solution in the presence of 0.3 mM xanthine, and the amorphous form in the absence/or presence of xanthine all show the high intensity of the (011) peak. However, when the ratios of intensity of (1−10)/(011), (020)/(011) and (−2−21)/(011) are calculated, then they decrease from 0.081, 0.199 and 0.186 to 0.056, 0.145 and 0.130, respectively. It is interesting to note that they all decrease by about

30%. Furthermore, the variation of ratio intensity of PXRD has been shown to be an effective evidence to elucidate the subtle changes in the nucleation and crystallization process.[25–27] Hence, this result further clarifies that the main inhibitory effect of xanthine is to disturb and suppress the three-dimensional crystallization process.

Understanding the mechanism of nucleation inhibition

Based on the above observations in solutions (DFT calculations, DLS, HNMR, and induction time results) and the reconfirmation of the detection on amorphous form of MSUM in the presence/absence of TMI (FTIR, Raman spectra, and PXRD), the mechanism of nucleation inhibition by xanthine in a solution, could be attributed to the following three aspects. Firstly, it could be accounted for not classical nucleation theory but the non-classical prenucleation phenomena (*e.g.*, ordering and aggregation), which, happening before the formation of the well-structured nuclei in solution, play a great role in affecting the nucleation process.[28] Secondly, xanthine could only inhibit the assembly of the FCSS and the growth of FCST in a specific direction in solution, so FCST could continue to develop into a planar in other directions, but its size would be reduced. Thirdly, as shown in Fig. 6, FCST could act as an "imposter" of FCSS to binding the (011) by the aromatic stacking interactions between the urate in the structure of FCST and urate in (011) plane, while xanthine in FCST causes a large binding barrier between the two (011) planes and the reduction in cluster size in solution. This special binding obstacle brings about an amplifying impact of inhibition, leading to a very huge inhibitory effect of a small amount of inhibitor, which could further explain the significant and unreasonable fluctuations of the pre-exponential parameter A. To the best of our knowledge, the nucleation inhibition of TMI is achieved by suppressing interplanar stacking, which is a mechanism to be proposed at the first time.
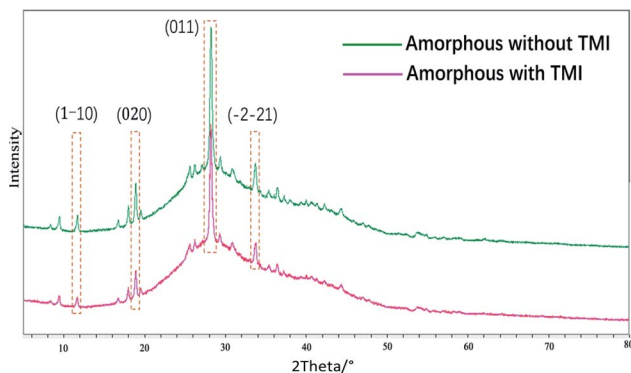

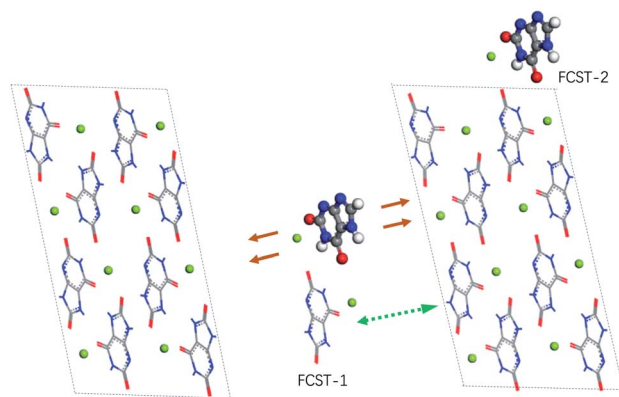**Fig. 5** PXRD patterns of the amorphous form of MSUM in the absence/presence of TMI.

Fig. 6 Proposed mechanism of nucleation inhibition caused by FCST in a solution. A green arrow indicates that the urate of FCST-1 is attracted to the (011) plane by aromatic stacking interactions, and the red arrows indicate that xanthine in FCST-1 exerts a repulsive force with the (011) plane to further prevent docking. Meanwhile, the FCST-2 presents that xanthine could only block the growth of (011) in a specific direction

Conclusions

This study, by means of DLS, HNMR, IR, Raman, PXRD, induction time measurements, and DFT calculations in the presence/absence of xanthine, revealed that the inhibition came from a combination of kinetic and thermodynamic effects, with an impact of kinetics as the TMI inhibition effects far exceeded what could be accounted for by changes in solubility and or other usual factors in classical nucleation theory. And these results demonstrated that the complexes between urate and TMI ion disturbed the formation of two-dimensional sheets of sodion and purine rings parallel to the (011) plane and further impeded the formation of three-dimensional structure. To our knowledge, the nucleation inhibition of TMI is achieved by suppressing interplanar stacking, which is a mechanism to be proposed at the first time.

Conflicts of interest

There are no conflicts to declare.

Acknowledgements

Notes and references

1 N. Dalbeth, T. R. Merriman and L. K. Stamp, *Lancet*, 2016, **388**, 2039–2052.
2 R. Pascal and B. Thomas, *Lancet*, 2010, **375**, 318–328.
3 J. Ulrich, *Chem. Eng. Technol.*, 2003, **26**, 832–835.
4 J. Chung, I. Granja, M. G. Taylor, G. Mpourmpakis, J. R. Asplin and J. D. Rimer, *Nature*, 2016, **536**, 446–450.
5 L. Hu, Y. Yang, H. Aloysius, H. Albanyan, M. Yang, J. J. Liang, A. Yu, A. Shtukenberg, L. N. Poloni, V. Kholodovych, J. A. Tischfield, D. S. Goldfarb, M. D. Ward and A. Sahota, *J. Med. Chem.*, 2016, **59**, 7293–7298.
6 C. A. P. Siepermann, S. Huang and A. S. Myerson, *Cryst. Growth Des.*, 2017, **17**, 2646–2653.
7 C. A. P. Siepermann and A. S. Myerson, *Cryst. Growth Des.*, 2018, **18**, 3584–3595.
8 P. L. Kaskiewicz, I. Rosbottom, R. B. Hammond, N. J. Warren, C. Morton, P. J. Dowding, N. George and K. J. Roberts, *Cryst. Growth Des.*, 2021, **21**, 1946–1958.
9 Y. Liu, R. Cheng, C. Ou, X. Zhang and T. Fu, *Cryst. Growth Des.*, 2020, **20**, 2842–2846.
10 Y. Liu, J. Jing, C. Ou, X. Zhang, S. Jiang, R. Chen and T. Fu, *CrystEngComm*, 2019, **21**, 3774–3778.
11 S. Jiang and J. H. Horst, *Cryst. Growth Des.*, 2011, **11**, 256–261.
12 M. J. Frisch, *et al.Gaussian 09*, Gaussian Inc., Wallingford, CT, 2009.
13 I. Kippen, J. R. Klinenberg, A. Weinberger and W. R. Wilcox, *Ann. Rheum. Dis.*, 1974, **33**, 313–317.
14 A. Da, A. Ren, R. Cheng, X. Zhang, Y. Pan, C. Ou, T. Fu and Y. Liu, *Crystengcomm*, 2021, **23**, 8411–8417.
15 D. Kashchiev and G. M. van Rosmalen, *Cryst. Res. Technol.*, 2003, **38**, 555–574.
16 I. Souvignet and S. V. Olesik, *Anal. Chem.*, 1998, **70**, 2783–2788.
17 M. Li, S. Li, W. Tang and J. Gong, *Cryst. Growth Des.*, 2020, **20**, 804–812.
18 D. Attwood, R. Waigh, R. Blundell, D. Bloor, A. Thévand, E. Boitard, J. P. Dubès and H. Tachoire, *Magn. Reson. Chem.*, 1994, **32**, 468–472.
19 K. Wolinski, J. F. Hinton and P. Pulay, *J. Am. Chem. Soc.*, 1990, **112**, 8251–8260.
20 D. Flaig, M. Maurer, M. Hanni, K. Braunger, L. Kick, M. Thubauville and C. Ochsenfeld, *J. Chem. Theory Comput.*, 2014, **10**, 572–578.
21 I. Weissbuch, M. Lahav and L. Leiserowitz, *Cryst. Growth Des.*, 2003, **3**, 125–150.
22 B. B. Parekh, S. R. Vasant, K. P. Tank, A. Raut, A. D. Vaidya and M. J. Joshi, *Am. J. Infect. Dis.*, 2009, **5**, 232–237.
23 S. Ahmed, M. M. Hasan and Z. A. Mahmood, *Pak. J. Pharm. Sci.*, 2017, **30**, 2101–2108.
24 N. N. Mafy, T. Afrin, M. M. Rahman, M. Y. A. Mollah and M. A. B. H. Susan, *RSC Adv.*, 2015, **5**, 59263–59272.
25 S. Xu, D. Cao, Y. Liu and Y. Wang, *Cryst. Growth Des.*, 2022, **22**, 2001–2022.
26 S. Castro-Garcia, A. Castro-Couceiro, M. Senaris-Rodriguez, A. F. Soulette and C. Julien, *Solid State Ionics*, 2003, **156**, 15–26.
27 G. G. Amatucci, J. M. Tarascon, D. Larcher and L. C. Klein, *Solid State Ionics*, 1996, **84**, 169–180.
28 D. Gebauer, M. Kellermeier, J. D. Gale, L. Bergstro and H. Colfen, *Chem. Soc. Rev.*, 2014, **43**, 2348–2371.